LOAD TEST ON UNREINFORCED MASONRY SHELL

NEBOJŠA MOJSILOVIĆ[1], ROMAN SCHNEIDER[2], SEBASTIAN VILLIGER[3] AND PETER MARTI[4]

[1]Senior Scientist, Institute of Structural Engineering, ETH Zurich, Switzerland
[2,3]B. Sc. Student of Civil Engineering, ETH Zurich, Switzerland
[4]Professor, Institute of Structural Engineering, ETH Zurich, Switzerland

SUMMARY

According to the recent teaching reform at ETH Zurich, students are strongly encouraged to participate in experimental research. Within the scope of a research project on the structural behaviour of unreinforced masonry shells a load test on a conoid-type shell made of model clay bricks was performed at ETH's Institute of Structural Engineering. This paper presents the results of the load test, discusses the structural behaviour of the shell and provides a set of conclusions as well as recommendations for future research.

INTRODUCTION

As exemplified in a most fascinating and elegant way by Eladio Dieste's work (Anderson 2004), structural masonry has a considerable potential for the construction of shells. Due to their negligible tensile strength unreinforced masonry shells have to be shaped such that they can resist the applied loads primarily by compressive membrane action. As part of a research project aiming at an improved understanding and an increased application of masonry shells a load test on a conoid-type shell made of model clay bricks was performed within the framework of the junior authors' bachelor thesis (Schneider and Villiger 2007).

MATERIAL TESTS

Model clay bricks with dimensions of 42.4x21.3x9.5 mm (average values obtained from 30 measurements) and a gross density of 1421 kg/m^3 were used, see Figure 1. In addition, a thin layer two-component epoxy mortar was used to produce 0.4 to 1 mm thick bed and head joints.

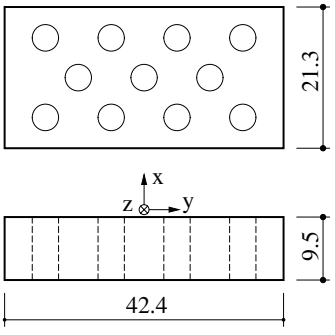

Figure 1. Model Clay Brick Unit (Dimensions in mm)

A set of standard tests were performed to obtain the masonry compressive strength perpendicular to the bed joints, f_x; the modulus of elasticity perpendicular to the bed joints, E_x; the masonry compressive strength parallel to the head joints, f_y; the modulus of elasticity parallel to the head joints, E_y; the masonry flexural strength perpendicular to the bed joints, f_{fx}; and the masonry flexural strength parallel to the head joints, f_{fy}, see Table 1 (Note: values refer to measured dimensions, which differed somewhat from nominal dimensions given in Figures 2 and 4). Mean values and standard deviations as well as 5% fractile values based on a confidence level of 95% (for the test series with five or more specimens) are given.

Table 1. Masonry Properties

	f_x [N/mm^2]	E_x [kN/mm^2]	f_y [N/mm^2]	E_y [kN/mm^2]	f_{fx} [N/mm^2]	f_{fy} [N/mm^2]
Number of tests	10	10	3	3	5	5
Mean value	43.0	20.3	18.8	15.8	11.8	9.9
Standard deviation	4.0	2.9	-	-	1.7	0.7
5% fractile value	36.4	15.5	-	-	9.0	8.8

Figures 2 (a) and (b) show the compression test specimens that were used to determine the compressive strengths and the moduli of elasticity perpendicularly to the bed and head joints, respectively. The load was applied by a universal testing machine with its lower head being fixed and its upper head being equipped with a ball joint. The load was applied steadily up to the failure of the specimen. Typically, failure occurred due to transverse splitting along the x-y plane.

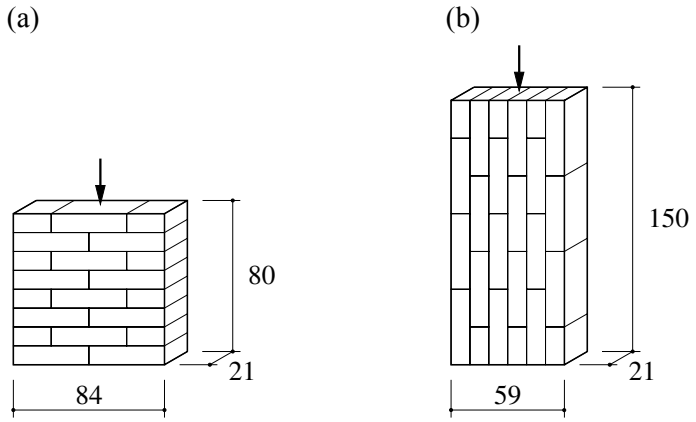

Figure 2. Compression Tests: (a) Determination of f_x and E_x; (b) Determination of f_y and E_y (Nominal Dimensions in mm)

Apart from the applied loads, strains were measured on one surface of the specimens using a video extensometer, see Figure 3. From additional strain gauge measurements and observations of the failure modes it was noticed in some tests to determine f_x and E_x that the load had an eccentricity of up to 1.5 mm. Such tests with high eccentricities were not considered for the average values reported in Table 1.

Figures 4 (a) and (b) show the bending test specimens that were used to determine the flexural strengths f_{fx} and f_{fy}, respectively. The load was applied by a universal testing machine in the form of a four-point bending test. The load was applied steadily up to the failure of the

specimen. The load was introduced by means of two steel rolls wrapped by neoprene sleeves with a diameter of 10 mm. The failure occurred due to rupture of the specimen along the joints and partly, even in the tests for determining f_{fx}, through the bricks.

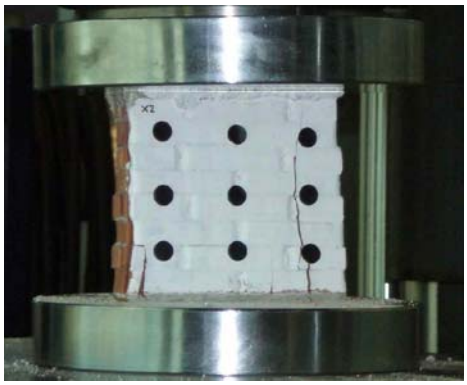

Figure 3. Video Extensometer Measurements on Specimen Surface

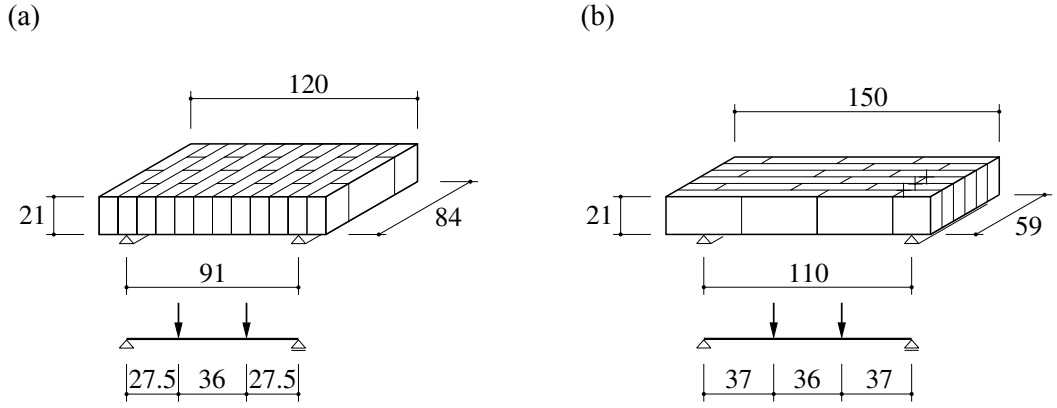

Figure 4. Bending Tests: (a) Determination of f_{fx}; (b) Determination of f_{fy} (Nominal Dimensions in mm)

SHELL GEOMETRY AND NUMERICAL ANALYSIS

A parabolic conoid was chosen for the shell shape, see Figure 5, i.e. a single curvature shell surface generated by a straight line *i* moving in such a manner as always to meet a given straight line *l* and a given parabola *p*, continuing parallel to a given plane δ.

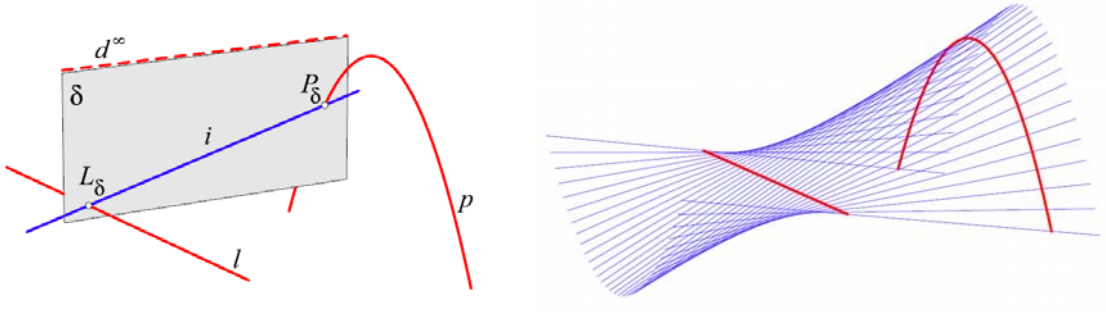

Figure 5. Parabolic Conoid with Directrices (Filipan et al. 2002)

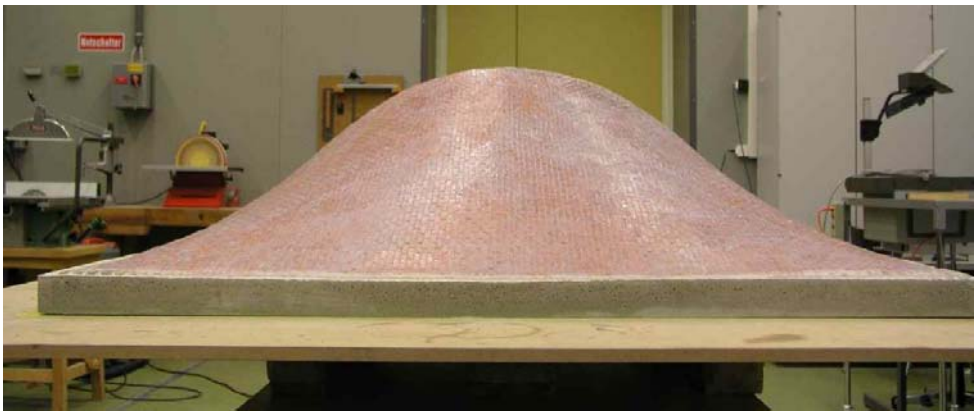

Figure 6. Back View of Masonry Shell

The shell spanned over a square plan with dimensions of 1.25x1.25 m. The quadratic parabola Directrix *p* of Figure 5 had a rise of 0.4 m, see Figure 6. The shell was vertically supported and horizontally restrained along the three horizontal (straight) edges and free along the parabolic edge.

A numerical analysis was performed using a standard commercial finite element program, assuming a linearly elastic response of a shell. The masonry was modelled as a homogeneous and isotropic material having a modulus of elasticity of 20 kN/mm^2 and a Poisson's ratio of 0.2. Three load cases were investigated: (i) uniformly distributed load of 0.3 kPa; (ii) 16 unit loads placed symmetrically about both axes, spaced at 305 mm; and (iii) 16 similarly arranged loads of 1 kN introduced via square loading areas of 100 mm side length. Figure 7 shows the stress distribution at the bottom (left) and top (right) specimen surfaces for Load Case 2. The highest tensile and compressive stresses are coloured blue and red, respectively. The calculated stresses and displacements were useful in deciding where to place the measurement devices, i.e. strain gauges and linearly variable displacement transducers (LVDTs).

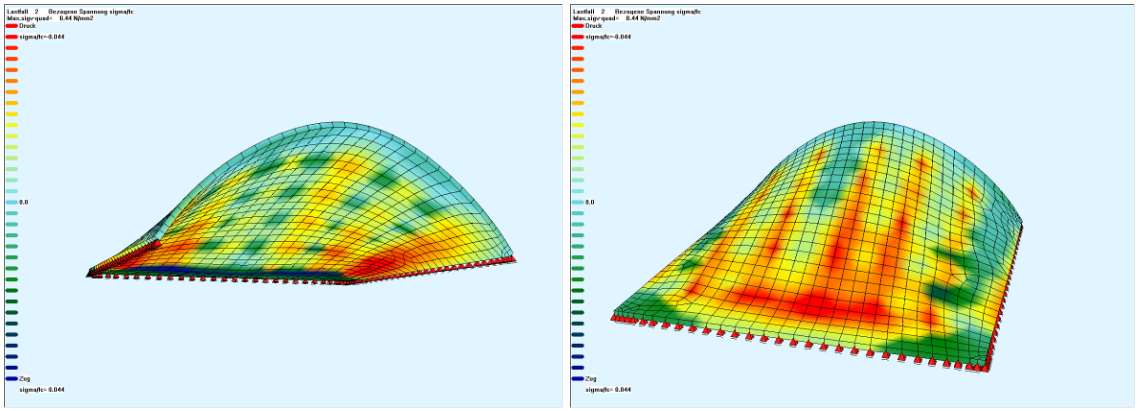

Figure 7. Stresses for Load Case 2

SHELL TEST

The shell was constructed using a wooden scaffolding as shown in Figure 8 (a), covered by 4 mm thick plywood boards, see Figure 8 (b). The plywood boards were covered with a

polyethylene film to avoid contact with the epoxy mortar. The shell was built in three stages, starting with the middle part, see Figure 8 (c). At the supported edges small beams were built using construction grout to ensure the proper boundary conditions in the test set-up.

(a) (b) (c)

Figure 8. Shell Construction: (a) Scaffolding; (b) Plywood Boards; (c) First Construction Stage

After construction, the shell was placed into the test set-up (see Figure 9 (a)) and the load application system was installed. The load was applied by means of 16 steel rods with a diameter of 6 mm which were connected to a rigid steel frame. This frame was flexibly attached to a hydraulic jack, see Figure 9 (b). Figure 9 (c) shows a detail of the load introduction into the shell. Square steel bearing plates with dimensions of 0.1x0.1 m were placed on the top of an epoxy layer in order to achieve the exact position of the plates and to ensure a proper load distribution. In addition, half-circular steel cylinders were used to avoid skew angle contacts between the rods and the bearing plates in the high curvature areas of the shell. In this way, a uniformly distributed load was simulated.

(a) (b) (c)

Figure 9. Test Set-up: (a) Supports; (b) Loading Frame; (c) Load Application on Top of Shell

Apart from the jack load, which was applied in a deformation-controlled manner, measurements included deflections at seven points and strains on both shell surfaces (see Figure 10 (a)). On the bottom surface one strain gauge rosette (R1) was placed. At the top surface, a corresponding rosette (R2) was placed in order to investigate the bending deformation. In addition, four strain gauges, S0 to S3, two in each direction, were placed on the top surface. Figure 10 (b) gives an overview of the deflection measurements, D1 to D7, which were acquired by means of LVDTs. The LVDTs were fastened to the steel profiles, which in turn were attached to the test frame. All measurement devices were connected to a personal computer which processed the acquired data in real time.

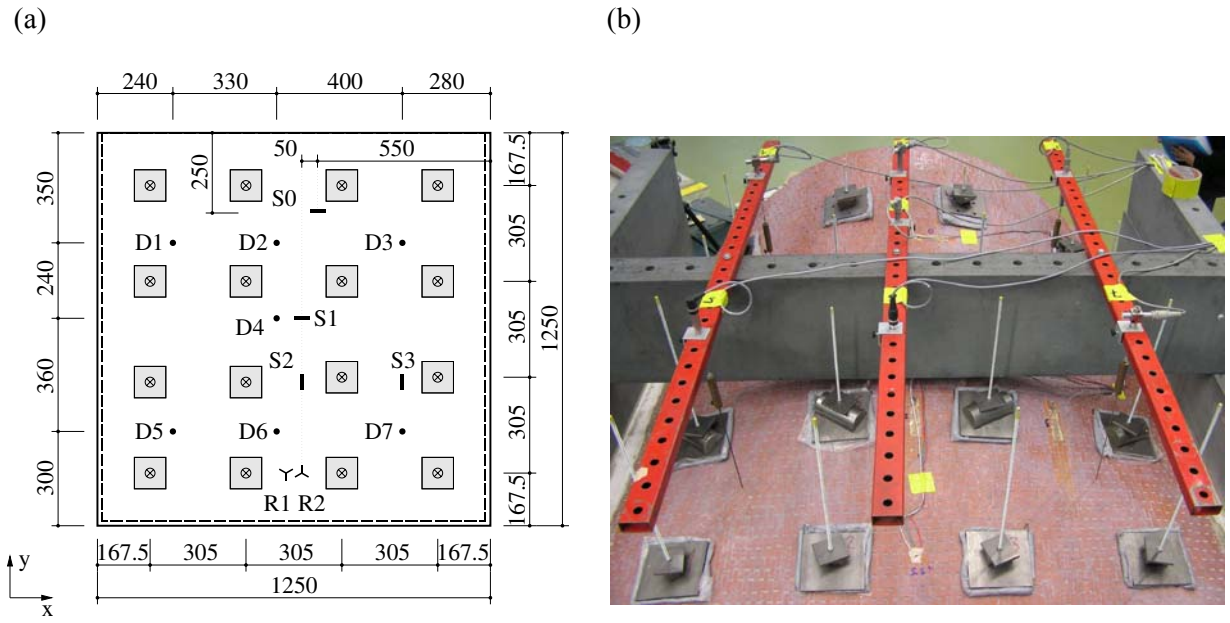

Figure 10. Measurements: (a) Overview; (b) LVDTs

TEST RESULTS

Figure 11 (a) shows the overall relationships between the total applied force and the seven deflections, D1 to D7. Figure 11 (b) depicts the early phase where a linearly elastic behaviour can be assumed.

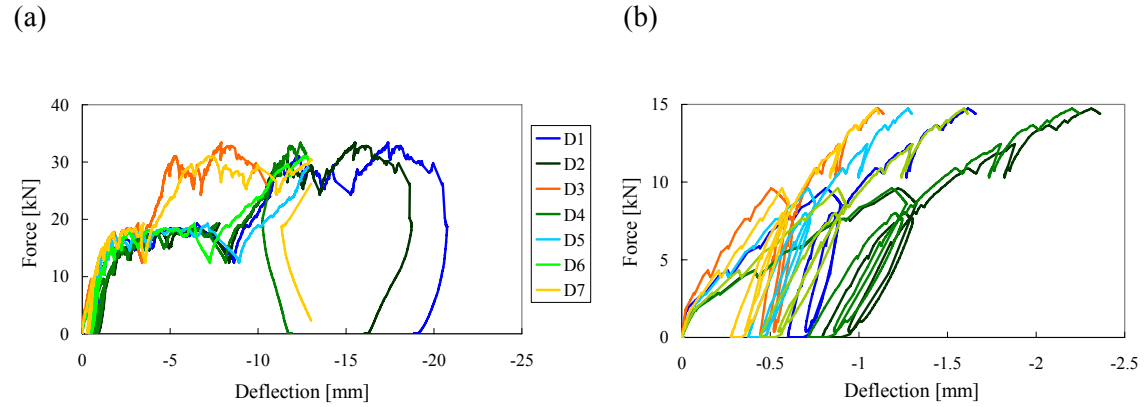

Figure 11. Force-Deflection-Relationships: (a) Overall Diagrams; (b) Initial Test Phase

It can be seen that the shell was not loaded symmetrically, i.e. the jack force was not equally distributed to the 16 steel rods. Even initially, the deflections D1 and D5 were larger than those on the opposite side of the shell, i.e. D3 and D7, see Figure 10 (b). Furthermore, after unloading from a load of approximately 9 kN the deflections did not recover completely, indicating a drifting of the side supports. This drifting was actually observed during the test.

Figure 12 illustrates the deformations and cracks in the shell immediately after reaching the peak load of about 34 kN. Two sagging cracks (tension at the bottom surface) occurred in the front part of the shell where an arching action in x-direction can be assumed. These cracks

confirm the fact that the supports drifted somewhat apart. Otherwise, for an arch failure mechanism, four plastic hinges would be needed and one of the two internal hinges would have to be hogging (tension at the top surface).

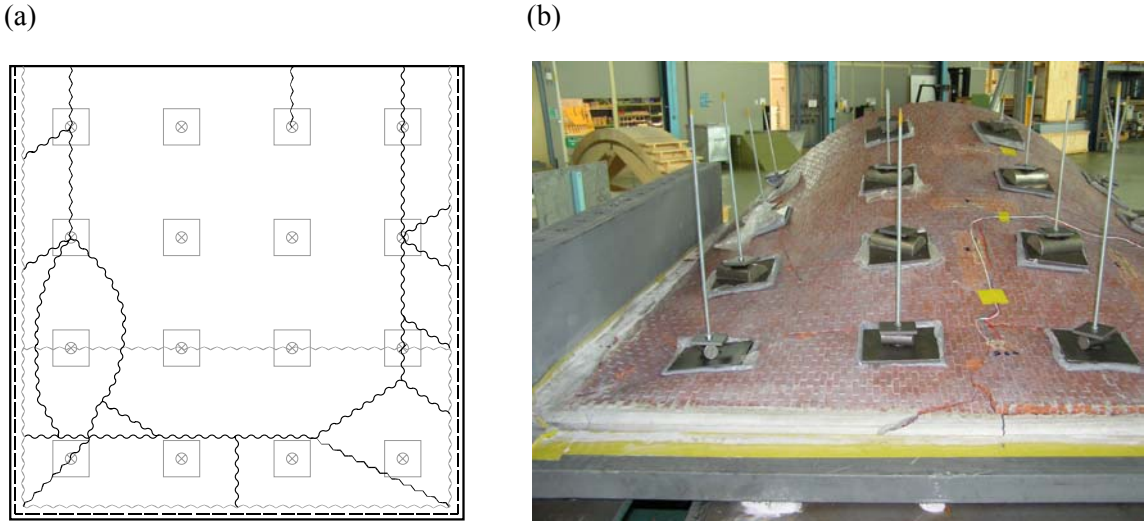

Figure 12. Shell Deformations: (a) Crack Pattern; (b) Failure Mechanism

DISCUSSION

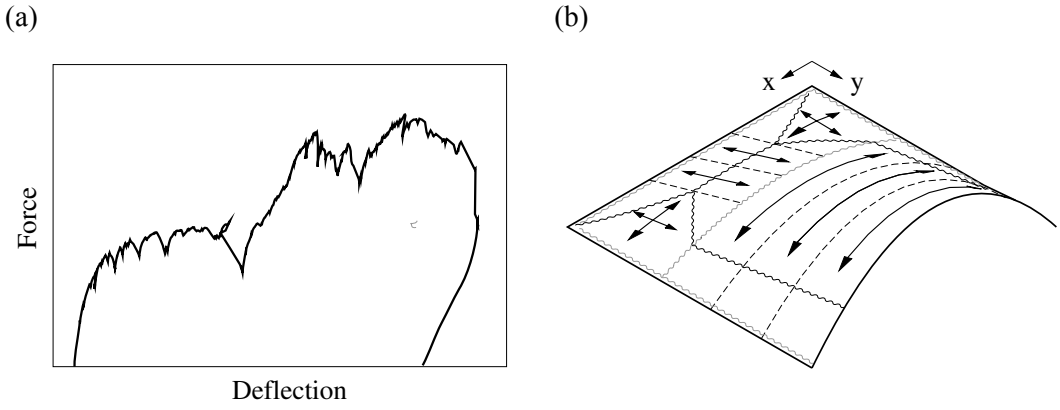

Figure 13. Structural Behaviour: (a) Generalised Force-Deflection-Characteristic; (b) Simplified Structural Model

Figure 13 shows a generalised force-deflection-characteristic (a) and a simplified structural model (b) taking into account the failure mechanism of the shell. After an initial linearly-elastic phase, the force-deflection curve reached a first plateau. Along the first plateau cracking became visible and audible. After this phase a second load increase took place, interrupted by the failure of the back part of the shell. In this phase, with a second load-deflection plateau developing, the back part of the shell acted like a plate in bending see Figure 13 (b). The peak load of 32 kN can be approximated by a simple analysis assuming that the back part is clamped into the front part, which in turn acts as an arch. Considering the clamped edge to lie at a distance of 472.5 mm from the simply supported back edge the single rod loads Q acting at a distance of 167.5 mm from the back edge produce average positive (negative) peak moments of 0.269 Q (-0.240 Q) over effective widths of 305 mm according to

a linearly elastic analysis, see Figure 10 (a). Assuming a lower characteristic flexural strength of 70% of the mean value $f_{fy} = 9.9$ N/mm^2 reported in Table 1 the characteristic flexural resistance per unit length equals $0.7 \cdot 9.9 \cdot 21^2/6 = 509$ N thus $Q = 509/0.269 = 1891$ N and $16Q = 30.3$ kN. Note that the reduction coefficient of 70% for the characteristic value is equal to that used for the similarly brittle concrete tensile strength (SIA 262, 2003).

After the failure of the back part, the load could be increased to a maximum of 34 kN, leading to a third ascending branch of the force-deflection curve. In this phase, the load was distributed to 12 rods only i.e. the load was carried solely by arching action in the front part of the shell, see Figure 13 (b).

CONCLUSIONS

Curved unreinforced masonry structures, such as the tested shell are capable of resisting a considerable load by compressive membrane action.

A simple structural model was successfully applied to analyse the structural behaviour of unreinforced masonry conoid-type shell subjected to (quasi) uniformly distributed load. This model divides the shell into two parts, i.e. the back part acting as a plate in bending and the front part carrying the load through arching action.

Future research on unreinforced masonry shells should concentrate on large-scale, if possible full-scale tests. Furthermore, an effort should be made to find optimum shapes for unreinforced masonry shells. Finally, the numerical modelling of masonry deserves more study.

ACKNOWLEDGMENTS

The model bricks were obtained from Ziegelei Rapperswil and the thin layer mortar was sponsored by Sika Schweiz AG. This support is gratefully acknowledged.

REFERENCES

Anderson, S. (Editor), "Eladio Dieste, Inovation in Structural Art", *Princeton Architectural Press*, New York, 2004, 264 pp.

Filipan, S., Gorjanc, S. and Kvasnicka, H., "Roofing with Parabolic Conoid (in Croatian)", *KoG - Scientific and Professional Information Journal of Croatian Society for Constructive Geometry and Computer Graphics*, Vol. 5, No. 5, 2002, pp. 57-64.

Schneider, R., and Villiger, S., "Test on Model Clay Brick Masonry Shell (in German)", B. Sc. thesis, *Institute of Structural Engineering*, ETH Zurich, Switzerland, 2007, 55 pp.

SIA 262, "Concrete Structures", Swiss Standard, *Swiss Association of Engineers and Architects*, Zurich, 2003, 90 pp.